



Precise Location of Passive Intermodulation in Long Cables by Fractional Frequency Based Multi-Range Rulers

DONG Anhua¹, LIANG Haodong², ZHU Shaohao²,
ZHANG Qi¹, ZHAO Deshuang¹

(1. University of Electronic Science and Technology of China, Chengdu 611731, China;
2. ZTE Corporation, Shenzhen 518057, China)

DOI: 10.12142/ZTECOM.202501013

<https://kns.cnki.net/kcms/detail/34.1294.TN.20250218.1313.002.html>,
published online February 18, 2025

Manuscript received: 2024-03-04

Abstract: A novel method is developed by utilizing the fractional frequency based multi-range rulers to precisely position the passive intermodulation (PIM) sources within radio frequency (RF) cables. The proposed method employs a set of fractional frequencies to create multiple measuring rulers with different metric ranges to determine the values of the tens, ones, tenths, and hundredths digits of the distance. Among these rulers, the one with the lowest frequency determines the maximum metric range, while the one with the highest frequency decides the highest achievable accuracy of the position system. For all rulers, the metric accuracy is uniquely determined by the phase accuracy of the detected PIM signals. With the all-phase Fourier transform method, the phases of the PIM signals at all fractional frequencies maintain almost the same accuracy, approximately 1° (about $1/360$ wavelength in the positioning accuracy) at the signal-to-noise ratio (SNR) of 10 dB. Numerical simulations verify the effectiveness of the proposed method, improving the positioning accuracy of the cable PIM up to a millimeter level with the highest fractional frequency operating at 200 MHz.

Keywords: passive intermodulation; location; multi-range

Citation (Format 1): DONG A H, LIANG H D, ZHU S H, et al. Precise location of passive intermodulation in long cables by fractional frequency based multi-range rulers [J]. *ZTE Communications*, 2025, 23(1): 101 - 106. DOI: 10.12142/ZTECOM.202501013

Citation (Format 2): A. H. Dong, H. D. Liang, S. H. Zhu, et al., "Precise location of passive intermodulation in long cables by fractional frequency based multi-range rulers," *ZTE Communications*, vol. 23, no. 1, pp. 101 - 106, Mar. 2025. doi: 10.12142/ZTECOM.202501013.

1 Introduction

Passive intermodulation (PIM) interference has become increasingly prominent with the growing demands for high-power, wideband, and multi-carrier microwave communication systems, such as high-speed 5G and 6G wireless communications, indoor distributed antenna systems, and satellite communications^[1]. PIM refers to the non-linear effect in high-power passive microwave devices due to the coupling mechanism of the electro-thermal and multi-physical fields. PIMs are generally generated as distorted products from the emitting of high-power signals or multi-carrier networks, which can interfere with the whole communication process and eventually weaken the performance of the communication systems^[2]. For a communication system, the PIM level has become an important technical index to evaluate the performance. Therefore, the strict PIM level is expected to minimize the interference and improve the system capacity. To obtain the limited PIM level and reduce the PIM interference efficiently, the generation mechanism of PIM interference has been first investigated. The results ob-

tained in Refs. [3 - 6] indicate that the PIM interference is usually generated by multiple physical factors causing shape alterations and imperfect connection, such as temperature and humidity, oxidation and pollution of clean surfaces, and loose connection of devices. PIM interference can be produced at the formed unknown sources that are formed within the radio frequency (RF) cables. Therefore, to further reduce PIM interference from the unknown PIM sources existing in the RF cables, the precise detection and location of PIM sources has attracted much interests.

Recently, the near-field scanning method has been used to detect the non-enclosed PIM source^[7]. Based on the field nephogram of the plane above the device under test (DUT), which is constructed using the measured amplitude and phase information of the magnetic field, the field nephograms of the plane below the DUT are estimated. From the estimated nephograms, the positions of the PIM sources can be located. Similarly, emission source microscopy (ESM) has been developed to locate PIM sources by measuring the amplitude and phase of the field on a plane a few wavelengths away from the DUT^[8]. Different

from the amplitude and phase information evaluated in Refs. [7] and [8], the position of PIM sources in the base station antenna is identified by the acoustic vibration method^[9], which detects the intensity of the modulated PIM signal. With the measured signals, another interesting method of the K-space multi-carrier signals is proposed to locate multiple PIM sources in microwave systems^[10]. However, the relatively low positioning accuracy of these methods needs to be improved.

In this paper, a high positioning accuracy method called fractional frequency based multi-range rulers (FF-MRR) has been developed to locate the PIM sources in RF cables precisely. The range of the PIM sources is obtained by processing each ranging datum of each fractional frequency signal. The diverse frequencies of ruler signals can be widely used across different scenarios without constructing complicated systems. The ruler signal is obtained by mixing a group of signals and the local oscillator signal in batches. Additionally, the proposed method is not limited by the narrow-band bandwidth because the fractional frequency signals can still be obtained by adjusting the local oscillator signal. With the adopted fractional frequencies, the higher frequency signals and the lower ones in the multi-range rulers can guarantee a high positioning accuracy and a long measured distance.

The remainder of this paper is as follows. The system model of FF-MRR for positioning the PIM sources is proposed in Section 2. The calculations of the precise location of PIM by FF-MRR are deduced in detail in Section 3. In Section 4, the numerical simulation results of locating the PIM sources by the proposed FF-MRR method are discussed and analyzed. Section 5 concludes the paper.

2 System Model of FF-MRR

Compared with the pulse method based on timing ranging, it is easier for the phase method based on phase ranging to achieve higher accuracy^[11]. However, the periodic ambiguity of phases makes the phase based methods difficult to precisely position PIM, when the cable length exceeds one wavelength of the detected signal. Fig. 1 shows the schematic diagram of a single metric ruler based locating system using the phase method, which calculates the location of the PIM source by multiplying half of the wavelength by the ratio obtained from dividing 2π by the measured phase. Based on such a metric ruler, the maximum measurement distance is limited to half of the signal wavelength. Although one can lower the signal frequency to increase the maximum measurement distance, the position accuracy will decrease.

To achieve both a long measurement distance and high positioning accuracy, we have developed a novel method called FF-MRR. In our proposed method, three fractional frequencies are employed to build multiple metric rulers with different measurement ranges. The metric ruler based on the lowest frequency is to obtain the maximum measurement range while the metric ruler based on the highest frequency is to increase the positioning accuracy. The metric ruler based on the middle frequency is designed to eliminate the periodic ambiguity of phases. In this study, we call them the long ruler, fine ruler, and short ruler.

Fig. 2 illustrates the proposed FF-MRR system and its components for locating the PIM source. In the system, a fractional frequency generator is employed to generate signals operating at specific frequencies. During the positioning process, the fractional signal is modulated onto the first channel signal, which will carry the useful message. After passing through the filter and being amplified by the power amplifier, the signal is combined with the amplified signal from the second channel by the combiner to form a double-tone signal. To obtain the reference PIM signal and the real PIM signal from the RF cable, a forward coupler and a backward coupler are inserted between the combiner and the RF cable. The forward coupler extracts a small amount of power from the double-tone signals to generate a reference PIM signal by a passive mixer. The backward coupler captures the PIM signals generated by the RF cable. For both the reference and real PIM signals, a down-converter is utilized to lower the frequency of the PIM signals so that we can apply a low-rate analog-to-digital converter (ADC) to collect the PIM signals. Such a design does not directly sample the PIM signals at very high frequencies, thereby reducing the cost and complexity of the positioning system. After ADC captures the real PIM signals and the reference, MCU will perform the program to extract the phase of the PIM signal operating at the fractional frequency. For each fractional frequency, the system performs the phase detection for the PIM signal.

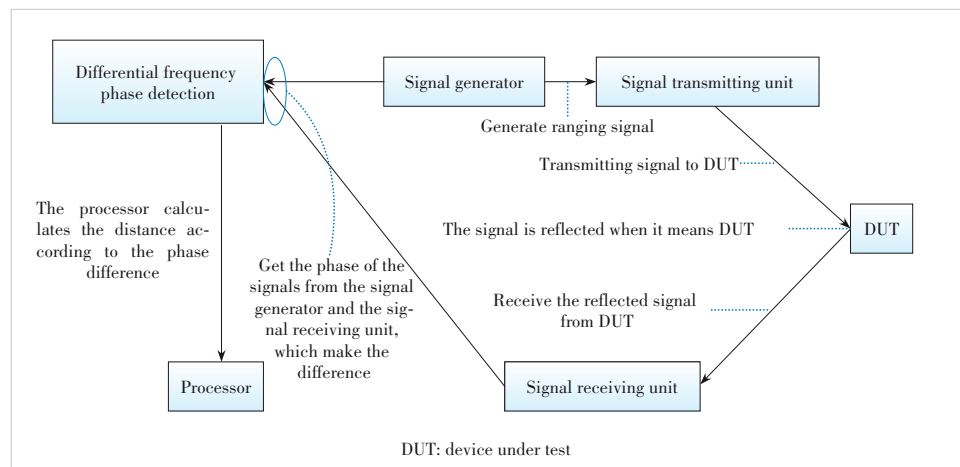


Figure 1. Schematic block diagram of a single ruler locating system

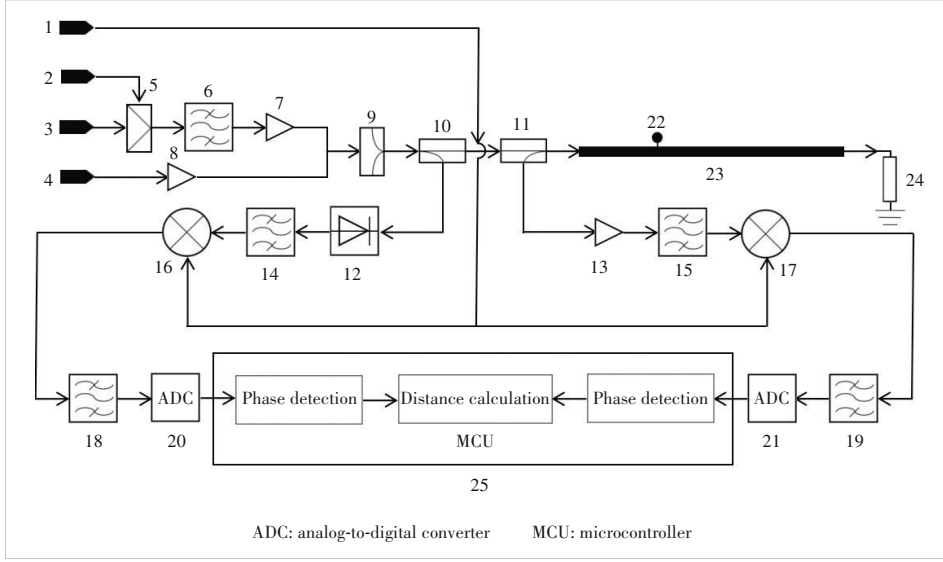


Figure 2. Block diagram of the FF-MRR system to locate PIM source. 1: local oscillator with f_{l0} , 2: fractional frequency control signal with f_0 , 3: the first signal source at f_1 , 4: the second signal source at f_2 , 5: modulator, 6: filter, 7 and 8: power amplifiers, 9: combiner, 10: forward coupler, 11: backward coupler, 12: passive mixer, 13: low noise amplifier, 14 and 15: filters, 16 and 17: down converters, 18 and 19: low pass filters, 20 and 21: analog-to-digital converters, 22: PIM source, 23: RF cable, 24: matching load, and 25: MCU

3 PIM Location with FF-MRR

3.1 Range Distance Based on Phase Differences

Assume that the frequencies of double-tone signals passing through the combination of two channels are f_1 and f_2 , and their initial phases are φ_1 and φ_2 , respectively. Moreover, the measured distance of the double-tone signals D_1 can be obtained by $f_s + f_s$:

$$D_1 = \frac{c}{2f_1} \frac{\varphi_1}{2\pi} = \frac{c}{2f_2} \frac{\varphi_2}{2\pi} \quad (1),$$

where c is the velocity of the electromagnetic wave. From Eq. (1), $\varphi_1 = \frac{4f_1\pi D_1}{c}$ and $\varphi_2 = \frac{4f_2\pi D_1}{c}$ can be acquired. The third-order intermodulation signal is generated by the two signals with f_1 and f_2 , whose frequency f_s is assumed as $f_s = 2f_1 - f_2$ with the initial phase $\varphi_s = 2\varphi_a - \varphi_b$. Similarly, the measured distance of the generated third-order intermodulation signal D_2 with the frequency f_s is formulated as:

$$D_2 = \frac{c}{2f_s} \frac{\varphi_s}{2\pi} = \frac{c}{2(2f_1 - f_2)} \frac{2\varphi_1 - \varphi_2}{2\pi} \quad (2).$$

By substituting $\varphi_1 = \frac{4f_1\pi D_1}{c}$ and $\varphi_2 = \frac{4f_2\pi D_1}{c}$ into Eq. (2), it can be reformulated as:

$$D_2 = \frac{c}{2(2f_1 - f_2)} \frac{4\pi D_1 (2f_1 - f_2)}{c} \frac{1}{2\pi} = D_1 \quad (3).$$

Eqs. (2) and (3) show that the measured distance depends on the phase differences caused by the transmission path.

3.2 Range Distance with FF-MRR

To locate the positions of the PIM sources, the phase difference from the third-order intermodulation signal caused by the transmission path should be first obtained. The referred PIM signal f_{IM3} generated by the double-tone signal with f_1 and f_2 is output from the forward coupler, which can be formulated as:

$$f_{IM3} = A_{IM3} \cos [2\pi(2f_1 - f_2 - 2f_0)t + (2\varphi_1 - \varphi_2 - 2\varphi_0)] \quad (4),$$

where A_{IM3} is the amplitude of the referred PIM signal, and f_0 and φ_0 are the frequency and initial phase of the ruler control signal.

The double-tone signals are input into the cable to be tested and transmitted to the position of the PIM source within Δt . Then, the double-tone signal undergoes nonlinear intermodulation, resulting in an intermodulation signal with the same frequency as the referred third-order intermodulation signal f_{IM3} . With the phase differences caused by the transmission path, the reflected intermodulation signal f'_{IM3} at the input port is received, which can be obtained by:

$$f'_{IM3} = A_{IM3} \cos [2\pi(2f_1 - f_2 - 2f_0)t + 2(\varphi_1 - \varphi_0) - \varphi_2 + 2 \cdot 2\pi(2f_1 - f_2 - 2f_0)\Delta t] \quad (5).$$

The phase differences φ_{IM3} caused by the transmission path can be obtained by:

$$\varphi_{IM3} = 2\pi(2f_1 - f_2 - 2f_0)(2\Delta t) \quad (6).$$

Based on the measured phase discrimination accuracy of 1° , the ranges of wavelengths of the long ruler, fine ruler, and short ruler are $200 \text{ m} \leq \lambda_L \leq 360 \text{ m}$, $2 \text{ m} \leq \lambda_F \leq 36 \text{ m}$, and $0.2 \text{ m} \leq \lambda_S \leq 3.6 \text{ m}$, respectively. Correspondingly, the ranges of frequencies of the long ruler, fine ruler, and short ruler are $0.42 \text{ MHz} \leq f_L \leq 1.5 \text{ MHz}$, $4.2 \text{ MHz} \leq f_F \leq 150 \text{ MHz}$ and $42 \text{ MHz} \leq f_S \leq 1500 \text{ MHz}$, respectively. From the long ruler, the coarse distance D_L can be obtained by:

$$D_L = c \frac{\varphi_L}{4\pi f_L} \quad (7),$$

where $\varphi_L = \varphi_{IM3}$ is measured by MCU in Fig. 2. From the fine

ruler, the relative accurate range distance D_F can be obtained by:

$$\begin{cases} D_F = c \frac{\varphi_F + 2\pi K_F}{4\pi f_F} \\ K_F = \left[\frac{D_L - c\varphi_F/4\pi f_F}{\lambda_F} \right]_{\text{int}} \end{cases} \quad (8),$$

where φ_F is measured by MCU in Fig. 2, K_F is an integer from the fine ruler, and $[\]_{\text{int}}$ is the integer operator. More accurately, from the short ruler, the precise range distance D_S can be obtained by:

$$\begin{cases} D_S = c \frac{\varphi_S + 2\pi K_S}{4\pi f_S} \\ K_S = \left[\frac{D_F - c\varphi_S/4\pi f_S}{\lambda_S} \right]_{\text{int}} \end{cases} \quad (9),$$

where φ_S is also measured by MCU in Fig. 2, and K_S is an integer from the short ruler. Finally, the final measured distance of the PIM source D_{IM3} can be obtained from the most precise range distance, which can be formulated as

$$D_{\text{IM3}} = D_S \quad (10).$$

4 Simulation Results of PIM Location

4.1 Simulation Setup

The specific simulation conditions are set as shown in Tables 1 and 2.

According to the project requirements, the specified transmission frequency band ranges from 1 805 MHz to 1 880 MHz. Consequently, the setup of f_1 and f_2 has adopted two frequencies in the transmission band, namely 1 820 MHz and 1 880 MHz. In fact, this system is basically not limited by the frequency band and bandwidth. By adjusting the local oscillator signal f_{l_0} , this system can be adaptable to frequency bands and bandwidths under various conditions. The positioning accuracy of PIM through FF-MMR depends on the highest fractional frequency in the fractional frequency based multi-range rulers. By adjusting the fractional frequency control signal with f_0 , it

Table 1. Setup of frequency-related conditions in the simulation

First Signal Source f_1 /MHz	Second Signal Source f_2 /MHz	Highest Fractional Frequency f_f /MHz	Fractional Frequency Control Signal f_0 /MHz	Local Oscillator Signal f_{l_0} /MHz
1 820	1 880	200	780	190

Table 2. Setup of other conditions in the simulation

Relative Dielectric Constant of Cable	Signal-to-Noise Ratio/dB	Phase Discrimination Accuracy/(°)
2	10	1

is easy to reach the fractional frequency up to 200 MHz or even higher. Therefore, a conservative setup of 200 MHz is adopted for f_s here. f_0 is calculated based on the configured values of f_1 , f_2 , and f_s . The main function of the local oscillator signal f_{l_0} is to down-convert the reference signal and the actual PIM signal so that we can use a lower rate ADC to collect PIM signals. The project requires a receiver sampling rate of 92.16 MHz. To make the sampling frequency close to 10 times the signal frequency, the local oscillator signal f_{l_0} is set to 190 MHz, so that the signal at the receiving end can be reduced to 10 MHz. The local oscillator signal f_{l_0} can be changed as needed based on actual requirements. Commonly seen on the market, the dielectric constant of radio frequency coaxial lines with foamed polyethylene (PE) as the dielectric layer is approximately between 1.4 and 2.0, while the ones with PE as the dielectric layer have a dielectric constant of around 2.3. Here, the relative dielectric constant of the cable is set to 2. For high-frequency signal transmissions, the signal-to-noise ratio usually needs to reach 15 dB or above. Here, a relatively poor communication environment (the SNR is assumed as 10 dB) has been chosen for simulation. Existing phase detection technologies generally can achieve phase detection accuracy in the millidegree range or higher. Here, a relatively conservative configuration of 1 degree is adopted for the phase detection accuracy.

4.2 Numerical Results

Table 3 shows the range distances for the PIM source by FF-MRR considering the highest fraction frequency f_s . Generally, the distances of PIM sources range from 0.1 m to 20 m. The columns “Error #1” to “Error #5” represent the average of ten independent and repeatable trials. A total of 14 distance ranging cases from PIM sources is conducted using FF-MRR, and an average ranging error of 0.490 mm is obtained, which

Table 3. Simulation ranging error of 200 MHz ruler signal under different distances to be measured

Distance/m	Error#1/mm	Error#2/mm	Error#3/mm	Error#4/mm	Error#5/mm	Average Error/mm
20	0.692	0.795	0.751	0.780	0.721	0.747 8
18	0.467	0.557	0.287	0.287	0.467	0.413 0
16	0.336	0.336	0.236	0.336	0.236	0.296 0
14	0.741	0.719	0.732	0.727	0.732	0.730 2
12	0.300	0.519	0.339	0.191	0.300	0.329 8
10	0.332	0.575	0.413	0.494	0.332	0.429 2
7	0.433	0.357	0.509	0.509	0.585	0.478 6
5	0.280	0.280	0.508	0.166	0.166	0.280 0
3	0.689	0.737	0.737	0.717	0.746	0.735 2
1	0.504	0.262	0.357	0.452	0.357	0.386 4
0.7	0.259	0.259	0.450	0.641	0.641	0.450 0
0.5	0.658	0.710	0.710	0.658	0.658	0.678 8
0.3	0.780	0.693	0.564	0.607	0.607	0.650 5
0.1	0.174	0.399	0.286	0.174	0.286	0.263 8

is less than 1 mm. Furthermore, Table 4 provides a comparative analysis of the positioning accuracy of various technologies used for locating PIM sources. The proposed FF-MRR method achieves a positioning accuracy of approximately 1 mm, outperforming near-field scanning (10 mm), acoustic vibration (10 mm), K-space (37.5 mm) and ESM (5 mm). Consequently, the favorable errors of range distances indicate the precise location of PIM sources can be achieved by FF-MRR compared with the other positioning technologies.

4.3 Errors Analysis

Moreover, the SNR and transmission velocity from filters, mixers and other components affecting the positioning error should be analyzed in the real measured environment.

Firstly, noise interference is considered in the positioning error, which is referred to as random Gaussian white noise. Fig. 3 shows the positioning error obtained by FF-MRR varies with the increased SNR. The maximum fractional frequencies of signals are considered as 7.5 MHz, 15 MHz, 30 MHz, 50 MHz, 100 MHz, 150 MHz and 200 MHz with the initial phase of 60 degrees. Additionally, the sampling frequency is 500 MHz. It can be found that a lower frequency results in a higher ranging error, because the ranging error is determined by the signal wavelength and the accuracy of the identification phase. When the accuracy of the identification phase remains unchanged, the longer the wavelength of the ranging signal, the greater the range error. Generally, as the SNR increases, the ranging errors decrease. The ranging error is declined to approximate 0.01 wavelengths when the SNR exceeds 10 dB with the frequency of ranging signal higher than 50 MHz.

Besides, the relative dielectric constant of transmission line can alter the velocity of electromagnetic wave, thereby influencing the ranging accuracy. Fig. 4 illustrates that the range errors vary with the relative dielectric constant of the transmission line. As the relative dielectric constant increases, the velocity of the electromagnetic wave decreases and the wavelength declines. Eventually, the ranging errors are reduced as well.

5 Conclusions

In this paper, an FF-MRR method is proposed to locate the PIM sources in cables. In the FF-MRR method, fractional frequency signals across multiple ranges can be obtained. Higher frequencies enable high-positioning accuracy, while lower fre-

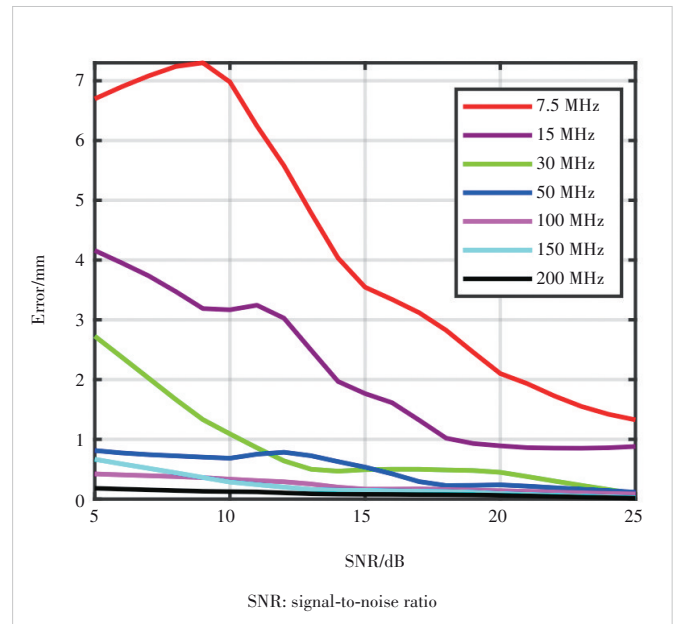


Figure 3. Positioning error versus SNR

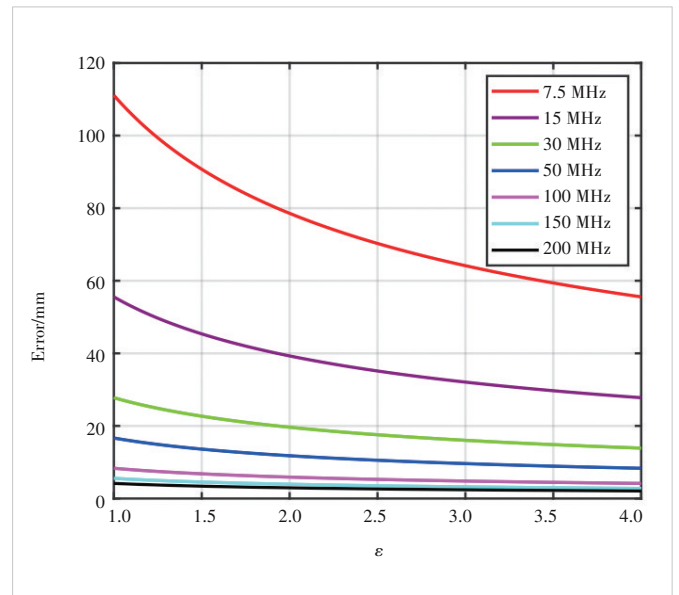


Figure 4. Influence of the relative dielectric constant of the RF cable on the positioning error at different fractional frequencies

quencies facilitate long range detection. Systematic simulations verify that the FF-MMR method has the advantage of high accu-

Table 4. Comparison of various PIM locating technologies

PIM Locating Technology	Scenario	Distance/m	Working Frequency/MHz	Error/mm
The near-field scanning ^[1, 12]	Microstrip line	0.21	935 - 960	10
Acoustic vibration ^[1, 9]	Antenna	-	1 850 - 1 990	10
K-space multi-carrier signals ^[10]	Cables	2.437	1 125 - 1 175	37.5
Emission source microscopy ^[8]	PCB	0.7	1 932 - 1 985	5
Our work	Cables	20	1 805 - 1 880	0.519

PCB: printed circuit board

PIM: passive intermodulation

rary. When the highest frequency is 200 MHz, the positioning accuracy can reach the millimeter level. Meanwhile, it only requires flexible adjustment of the wavelengths of the ruler signal to locate PIM sources with FF-MRR, which just needs a few seconds in the whole locating process, highlighting the high efficiency advantage of the method. In addition, the PIM source location approach using the FF-MRR method and the proposed system diagram employs a lower rate ADC without requiring other expensive instruments like scanning probes in near-field scanning methods. Therefore, this method also has the merits of lower cost and ease of portability. This method significantly improves the positioning performance in the PIM location technology for cable test scenarios compared with other methods. Nevertheless, the applicability of this method is somewhat restricted. It cannot be used in test scenarios involving antennas, printed circuit boards (PCBs), and the like.

References

- [1] CAI Z H, LIU L, DE PAULIS F, et al. Passive intermodulation measurement: challenges and solutions [J]. *Engineering*, 2022, 14: 181 – 191. DOI: 10.1016/j.eng.2022.02.012
- [2] ZHANG L, WANG H G, HE S T, et al. A segmented polynomial model to evaluate passive intermodulation products from low-order PIM measurements [J]. *IEEE microwave and wireless components letters*, 2019, 29(1): 14 – 16. DOI: 10.1109/LMWC.2018.2883719
- [3] WANG X L, CHEN X, SUN D Q. A compact contactless waveguide band-pass filter for high sensitivity passive intermodulation measurement [C]// *Proceedings of IEEE MTT-S International Wireless Symposium (IWS)*. IEEE, 2023: 1 – 3. DOI: 10.1109/IWS58240.2023.10223117
- [4] ISHIBASHI D, KUGA N. Numerical analysis of DUT-size effect on PIM measurement using standing-wave coaxial tube [C]// *Asia Pacific Microwave Conference*. IEEE, 2009: 2609 – 2612. DOI: 10.1109/APMC.2009.5385244
- [5] CANTALI G, DENIZ E, OZAY O, et al. PIM detection in wireless networks as an anomaly detection problem [C]// *International Balkan Conference on Communications and Networking (BalkanCom)*. IEEE, 2023: 1 – 6. DOI: 10.1109/BalkanCom58402.2023.10167980
- [6] WANG W B, WANG Y M, ZANG W X, et al. Physical mechanisms of passive intermodulation: a short review [C]// *International Applied Computational Electromagnetics Society Symposium (ACES-China)*. IEEE, 2022: 1 – 3. DOI: 10.1109/ACES-China56081.2022.10064913
- [7] XU Z. Research on electromagnetic interference source location algorithm based on near-field scanning [D]. Hangzhou: Zhejiang University, 2022. DOI: 10.27461/d.cnki.gzjdx.2022.000065
- [8] YONG S, YANG S, ZHANG L, et al. Passive intermodulation source localization based on emission source microscopy [J]. *IEEE transactions on electromagnetic compatibility*, 2020, 62(1): 266 – 271. DOI: 10.1109/TEMC.2019.2938634
- [9] YANG S, WU W, XU S, et al. A passive intermodulation source identification measurement system using a vibration modulation method [J]. *IEEE transactions on electromagnetic compatibility*, 2017, 59(6): 1677 – 1684. DOI: 10.1109/TEMC.2017.2705114
- [10] ZHANG M, ZHENG C, WANG X, et al. Localization of passive intermodulation based on the concept of K-space multicarrier signal [J]. *IEEE transactions on microwave theory and techniques*, 2017, 65(12): 4997 – 5008. DOI: 10.1109/TMTT.2017.2705099
- [11] LIU X H. Design of pulsed semiconductor laser ranging system [D]. Hohhot: Inner Mongolia University, 2014
- [12] SHITVOV P A, ZELENCHUK E D, SCHUCHINSKY G A, et al. Passive intermodulation generation on printed lines: near-field probing and observations [J]. *IEEE transactions on microwave theory and techniques*, 2008, 56(12): 3121 – 3128. DOI: 10.1109/TMTT.2008.2007136

Biographies

DONG Anhua received his BS degree from Jilin University, China in 2021. He is currently pursuing his ME degree at University of Electronic Science and Technology of China. His research interests include the positioning of radiated passive inter-modulation.

LIANG Haodong received his PhD degree in guidance, navigation and control from University of Electronic Science and Technology of China in 2021. He is currently an algorithm engineer at ZTE Corporation. His research interests include the modeling and positioning of passive inter-modulation.

ZHU Shaohao received his PhD degree in underwater acoustic engineering from Northwestern Polytechnical University, China in 2021. He is currently an RF algorithm engineer at ZTE Corporation. His research interests include PIM mechanism, PIM cancellation, source location, and array beamforming.

ZHANG Qi received his BS degree from Henan Polytechnic University, China in 2023. He is currently pursuing his ME degree at University of Electronic Science and Technology of China. His research interest focuses on the positioning of radiated passive intermodulation.

ZHAO Deshuang (dszhao@uestc.edu.cn) received his PhD degree in optical engineering from University of Electronic Science and Technology of China (UESTC), in 2005. He is currently a professor with the School of Physics, UESTC. His research interests include the modeling and positioning of conductor-guided and radiated passive intermodulation.